Transport through two-level quantum dots weakly coupled to ferromagnetic leads

I Weymann[1] **and J Barnaś**[1,2]

[1] Department of Physics, Adam Mickiewicz University, 61-614 Poznań, Poland
[2] Institute of Molecular Physics, Polish Academy of Sciences, 60-179 Poznań, Poland

E-mail: weymann@amu.edu.pl

Abstract
Spin-dependent transport through a two-level quantum dot in the sequential
tunnelling regime is analysed theoretically by means of a real-time
diagrammatic technique. It is shown that the current, tunnel magnetoresistance,
and shot noise (Fano factor) strongly depend on the transport regime, providing
detailed information on the electronic structure of quantum dots and their
coupling to external leads. When the dot is asymmetrically coupled to the leads,
a negative differential conductance may occur in certain bias regions, which is
associated with a super-Poissonian shot noise. In the case of a quantum dot
coupled to one half-metallic and one nonmagnetic lead, one finds characteristic
Pauli spin blockade effects. Transport may also be suppressed when the dot
levels are coupled to the leads with different coupling strengths. The influence
of an external magnetic field on transport properties is also discussed.

(Some figures in this article are in colour only in the electronic version)

1. Introduction

Quantum dots have already paved their way to become underlying devices of
magnetoelectronics and spintronics [1–4]—not only because of beautiful physics emerging
in those systems, but, more importantly, due to possible future applications and due to the
possibility of manipulation of a single spin [5–8]. The transport characteristics of quantum
dots coupled to nonmagnetic leads have already been extensively studied both theoretically and
experimentally. In nonmagnetic single-electron devices it is mainly the electron charge which
determines the system transport properties [9–12]. If, however, a quantum dot is coupled
to ferromagnetic leads, the transport characteristics strongly depend on the spin degree of
freedom, leading for example to the suppression of current when the alignment of magnetic
moments of the leads switches from parallel to antiparallel [13–15]. The difference between

the currents flowing through the system in these two magnetic configurations defines the so-called tunnel magnetoresistance (TMR).

Theoretical considerations of electronic transport through a quantum dot weakly coupled to ferromagnetic leads have been restricted mainly to single-level quantum dots. Transport properties of such systems have been analysed in the sequential tunnelling regime [15–17], as well as in the cotunnelling regime [18–20]. In real systems, however, usually more than one energy level participates in transport, leading to more complex and interesting transport characteristics [21–23]. Several experimental realizations of quantum dots attached to ferromagnetic contacts have already been reported, which include self-assembled dots in ferromagnetic semiconductors [24], ultrasmall metallic grains [7, 25], granular structures [26], carbon nanotubes [27–30], single molecules [31], or magnetic tunnel junctions [32].

In this paper we consider transport through two-level quantum dots coupled to ferromagnetic leads, and restrict our considerations to the sequential tunnelling regime. The dot is described by the Anderson-like impurity Hamiltonian. Thus, the analysis may also hold for some magnetic impurities and molecules. With the aid of the real-time diagrammatic technique, we calculate the current I, differential conductance G, and Fano factor F in the parallel and antiparallel magnetic configurations, as well as the corresponding TMR. The Fano factor, $F = S/S_p$, describes the deviation of the zero-frequency shot noise S from the Poissonian shot noise $S_p = 2e|I|$ (corresponding to uncorrelated electronic transport).

In the following we analyse the transport properties in two situations: (i) when the dot is symmetrically coupled to the leads, and (ii) when the dot is coupled asymmetrically to the leads. In both cases the transport characteristics are shown to be strongly dependent on the transport regime. As a result, the variation of TMR with the transport and gate voltages is significantly different from that for single-level quantum dots. Furthermore, the Fano factor is found to exhibit a nontrivial dependence on the magnetic configuration of the system and spin polarization of the leads. For symmetric coupling to ferromagnetic leads, the Fano factor becomes divergent in the parallel configuration when the leads' polarization tends to unity, while in the antiparallel configuration the shot noise is Poissonian. On the other hand, in the case of asymmetric coupling of the dot to external leads, we find transport regions where the current is (partly) suppressed. These transport regions are accompanied by negative differential conductance (NDC) and a super-Poissonian shot noise. If the dot is coupled to one half-metallic and one nonmagnetic lead, the blockade regions are associated with particular occupation of a dot spin state and can be referred to as the Pauli spin blockade regions. In addition, we also discuss the effect of an external magnetic field on the transport characteristics. The TMR displays then a rather complex behaviour with the bias voltage.

We note that such effects as spin blockade, NDC, sub- and super-Poissonian shot noise, and tunnel magnetoresistance also occur in single-level quantum dots [15, 16]. Although the physical mechanisms responsible for some of the above effects in two-level quantum dots are similar to those in single-level dots, the resulting transport characteristics in two-level dots are much more complex. The analysis of these effects in the case of two-level quantum dots coupled to ferromagnetic leads is the main objective of the present work.

The paper is organized as follows. In section 2 we describe the model. The method used to calculate the transport characteristics is presented briefly in section 3. Results of numerical calculations are shown and discussed in section 4, where we first consider the case of a quantum dot coupled symmetrically to the leads, and then analyse transport through quantum dots with unequal couplings. Section 4 also includes some approximate analytical expressions obtained for the most characteristic transport regions. The corresponding formulae may be useful in discussing future experiments. Finally, a summary and conclusions are given in section 5.
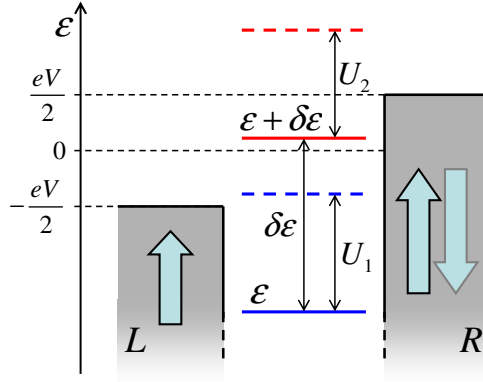
Figure 1. Energy diagram of a two-level quantum dot coupled to ferromagnetic leads. For clarity reasons the energy diagram is shown here for $\Delta = U' = 0$. However, in the paper we consider the case when the Coulomb interaction between electrons occupying different orbitals is described by a nonzero value of the parameter U'. The leads' magnetizations can form either parallel or antiparallel configurations. The arrows indicate the net spin of the leads.

2. Model

The system considered in this paper is shown schematically in figure 1 and consists of a quantum dot with two orbital levels coupled to ferromagnetic leads. The net spin moments of the leads are assumed to be collinear, i.e., they can form either parallel or antiparallel magnetic configuration, as indicated in figure 1. The Hamiltonian $\hat{H}$ of the system includes four terms: $\hat{H} = \hat{H}_{\mathrm{L}} + \hat{H}_{\mathrm{R}} + \hat{H}_{\mathrm{D}} + \hat{H}_{\mathrm{T}}$. The first two terms describe noninteracting itinerant electrons in the leads, $\hat{H}_r = \sum_{\mathbf{k}\sigma} \varepsilon_{r\mathbf{k}\sigma} c_{r\mathbf{k}\sigma}^{\dagger} c_{r\mathbf{k}\sigma}$ for the left ($r = \mathrm{L}$) and right ($r = \mathrm{R}$) leads, with $\varepsilon_{r\mathbf{k}\sigma}$ being the energy of an electron with the wavevector $\mathbf{k}$ and spin σ in the lead r, and $c_{r\mathbf{k}\sigma}^{\dagger}$ ($c_{r\mathbf{k}\sigma}$) denoting the respective creation (annihilation) operator. The quantum dot is described by the following Anderson-like Hamiltonian:

$$\hat{H}_{\mathrm{D}} = \sum_{j\sigma} \varepsilon_j n_{j\sigma} + \sum_j U_j n_{j\uparrow} n_{j\downarrow} + U' \sum_{\sigma\sigma'} n_{1\sigma} n_{2\sigma'} - \frac{\Delta}{2} \sum_j \left(n_{j\uparrow} - n_{j\downarrow} \right), \tag{1}$$

where $d_{j\sigma}^{\dagger}$ ($d_{j\sigma}$) is the creation (annihilation) operator of an electron with spin σ on the jth level ($j = 1, 2$), ε_j is the corresponding single-particle energy, and $n_{j\sigma}$ is the particle number operator, $n_{j\sigma} = d_{j\sigma}^{\dagger} d_{j\sigma}$. The on-level Coulomb repulsion between two electrons of opposite spins is described by U_j, whereas the inter-level repulsion energy is denoted by U'. The fourth term in equation (1) describes the Zeeman energy, with $\Delta = g\mu_{\mathrm{B}} B$ being the Zeeman splitting of the energy levels (B is an external magnetic field along the magnetic moment of the left electrode). To describe the energy structure of the dot we introduce the level spacing $\delta\varepsilon = \varepsilon_2 - \varepsilon_1$ and define $\varepsilon_1 \equiv \varepsilon$. Since the different orbital levels can couple differently to an applied magnetic field, $\delta\varepsilon$ can be controlled by changing the magnetic field [33], while ε can be tuned by a gate voltage.

Tunnelling processes between the dot and electrodes are described by the Hamiltonian

$$\hat{H}_{\mathrm{T}} = \sum_{r=\mathrm{L},\mathrm{R}} \sum_{\mathbf{k}j\sigma} \left(t_{rj} c_{r\mathbf{k}\sigma}^{\dagger} d_{j\sigma} + t_{rj}^{\star} d_{j\sigma}^{\dagger} c_{r\mathbf{k}\sigma} \right), \tag{2}$$

where t_{rj} denotes the tunnel matrix elements between the lead r and the jth dot level. Coupling of the jth level to external leads can be described by $\Gamma_{rj}^{\sigma} = 2\pi |t_{rj}|^2 \rho_r^{\sigma}$, with ρ_r^{σ} being

Table 1. The dot eigenstates $|\chi\rangle$ and their energies ε_χ.

χ	Eigenstates	Energies
1	$|0\rangle|0\rangle$	0
2	$|\uparrow\rangle|0\rangle$	$\varepsilon - \Delta/2$
3	$|\downarrow\rangle|0\rangle$	$\varepsilon + \Delta/2$
4	$|0\rangle|\uparrow\rangle$	$\varepsilon + \delta\varepsilon - \Delta/2$
5	$|0\rangle|\downarrow\rangle$	$\varepsilon + \delta\varepsilon + \Delta/2$
6	$|\uparrow\rangle|\downarrow\rangle$	$2\varepsilon + \delta\varepsilon + U'$
7	$|\downarrow\rangle|\uparrow\rangle$	$2\varepsilon + \delta\varepsilon + U'$
8	$|\uparrow\rangle|\uparrow\rangle$	$2\varepsilon + \delta\varepsilon + U' - \Delta$
9	$|\downarrow\rangle|\downarrow\rangle$	$2\varepsilon + \delta\varepsilon + U' + \Delta$
10	$|\uparrow\downarrow\rangle|0\rangle$	$2\varepsilon + U_1$
11	$|0\rangle|\uparrow\downarrow\rangle$	$2\varepsilon + 2\delta\varepsilon + U_2$
12	$|\uparrow\rangle|\uparrow\downarrow\rangle$	$3\varepsilon + 2\delta\varepsilon + U_2 + 2U' - \Delta/2$
13	$|\downarrow\rangle|\uparrow\downarrow\rangle$	$3\varepsilon + 2\delta\varepsilon + U_2 + 2U' + \Delta/2$
14	$|\uparrow\downarrow\rangle|\uparrow\rangle$	$3\varepsilon + \delta\varepsilon + U_1 + 2U' - \Delta/2$
15	$|\uparrow\downarrow\rangle|\downarrow\rangle$	$3\varepsilon + \delta\varepsilon + U_1 + 2U' + \Delta/2$
16	$|\uparrow\downarrow\rangle|\uparrow\downarrow\rangle$	$4\varepsilon + 2\delta\varepsilon + U_1 + U_2 + 4U'$

the spin-dependent density of states in the lead r. By introducing the spin polarization of the lead r, $p_r = (\rho_r^+ - \rho_r^-)/(\rho_r^+ + \rho_r^-)$, the coupling parameters Γ_{rj}^σ can be expressed as $\Gamma_{rj}^{+(-)} = \Gamma_{rj}(1 \pm p_r)$, with $\Gamma_{rj} = (\Gamma_{rj}^+ + \Gamma_{rj}^-)/2$. Here, Γ_{rj}^+ and Γ_{rj}^- describe the coupling of the jth level to the spin-majority and spin-minority electron bands, respectively. In general, each dot level may be coupled to the leads with a different strength. Moreover, the coupling strengths may be energy dependent. In this work, however, they are assumed to be constant within the electron bands. For example, in the case of experiments performed in the weak coupling regime by Kogan *et al* [34], the coupling strength was found to be of the order of tens of microelectronvolts.

3. Method

We analyse the spin-polarized sequential transport through a two-level quantum dot. The first-order tunnelling gives the dominant contribution to charge current for voltages above a certain threshold voltage and is exponentially suppressed in the Coulomb blockade regime. The effects due to higher-order tunnelling, e.g., cotunnelling [18, 35], are not included. Taking into account the two orbital levels of the dot results in 16 different dot states $|\chi\rangle$ ($|\chi\rangle = |\chi_1\rangle|\chi_2\rangle$, with $|\chi_j\rangle$ corresponding to the jth level), as listed in table 1. The system is symmetrically biased and we assume equal capacitive couplings to the left and right lead, so the dependence of the dot energy levels on the bias voltage may be neglected. The energies of the corresponding dot eigenstates are listed in table 1.

Transport is calculated with the aid of the real-time diagrammatic technique [36, 37, 18, 21]. The technique consists in a systematic perturbation expansion of the dot density matrix and the current operator in the dot–lead couplings Γ_{rj}. In order to calculate the stationary occupation probabilities, current, and shot noise in the lowest order in the dot–lead coupling, we follow the procedure developed in [37, 21], and introduce the respective self-energy matrices: $\mathbf{W}$, $\mathbf{W^I}$, $\mathbf{W^{II}}$. The matrix $\mathbf{W}$ contains self-energies with one arbitrary row χ_0 replaced by $(\Gamma, \ldots, \Gamma)$, which is due to the normalization of the probabilities, $\sum_\chi P_\chi = 1$. The elements $W_{\chi\chi'}$ of the matrix $\mathbf{W}$ describe the first-order tunnelling transitions between the

many-body dot states $|\chi\rangle$ and $|\chi'\rangle$. They are given by [21] $W_{\chi\chi'} = W^{\mathrm{L}}_{\chi\chi'} + W^{\mathrm{R}}_{\chi\chi'}$, where
$W^r_{\chi\chi'} = 2\pi \sum_\sigma \rho^\sigma_r [f_r(\varepsilon_\chi - \varepsilon_{\chi'}) | \sum_j t^\star_{rj} \langle \chi | d^\dagger_{j\sigma} | \chi' \rangle |^2 + [1 - f_r(\varepsilon_{\chi'} - \varepsilon_\chi)] | \sum_j t_{rj} \langle \chi | d_{j\sigma} | \chi' \rangle |^2]$
for $\chi \neq \chi'$, while $W^r_{\chi\chi} = -\sum_{\chi' \neq \chi} W^r_{\chi'\chi}$, with $f_r(\varepsilon) = 1/[e^{(\varepsilon - \mu_r)/k_{\mathrm{B}}T} + 1]$ and μ_r being
the electrochemical potential of lead r. The second matrix, $\mathbf{W^I}$, denotes the full self-energy
matrix with one *external* vertex, resulting from the expansion of the tunnelling Hamiltonian,
replaced by the current operator. Finally, the third matrix, $\mathbf{W^{II}}$, consists of self-energies with
two *external* vertices replaced by the current operator. The current operator $\hat{I}$ is defined as
$\hat{I} = (\hat{I}_{\mathrm{R}} - \hat{I}_{\mathrm{L}})/2$, with $\hat{I}_r = -\mathrm{i}(e/\hbar) \sum_{\mathbf{k}\sigma} \sum_j (t_{rj} c^\dagger_{r\mathbf{k}\sigma} d_{j\sigma} - t^\star_{rj} d^\dagger_{j\sigma} c_{r\mathbf{k}\sigma})$ being the current
flowing from the lead r to the dot. The elements of the matrices $\mathbf{W^I}$ and $\mathbf{W^{II}}$ can be expressed
in terms of $W_{\chi\chi'}$ as [21] $W^{\mathrm{I}}_{\chi\chi'} = [\Theta(N_{\chi'} - N_\chi) - \Theta(N_\chi - N_{\chi'})](W^{\mathrm{R}}_{\chi\chi'} - W^{\mathrm{L}}_{\chi\chi'})$ and
$W^{\mathrm{II}}_{\chi\chi'} = (1 - 2\delta_{\chi\chi'})W_{\chi\chi'}/4$, respectively, where $N_\chi = \sum_{j\sigma} n_{j\sigma}$ and $\Theta(x)$ is the step function.

In this paper we calculate transport in the first order with respect to tunnelling processes.
In the collinear configurations discussed here, one might also apply a simpler method based on
the master equations. However, we apply a more sophisticated technique, which enables easy
extensions to noncollinear magnetic configurations and facilitates including the influence of
second- and higher-order tunnelling processes [38]. Furthermore, the real-time diagrammatic
technique employed here allows one to calculate the current and shot noise in a fully systematic
way order by order in the dot–lead coupling strength.

Having calculated the respective matrices, the stationary probabilities can be determined
from the following equation,

$$(\mathbf{WP})_\chi = \Gamma \delta_{\chi\chi_0}, \tag{3}$$

where $\mathbf{P}$ is the vector containing the occupation probabilities. In turn, the sequential current
flowing through the system can be calculated from

$$I = \frac{e}{2\hbar} \mathrm{Tr}\{\mathbf{W^I P}\}, \tag{4}$$

with $\mathrm{Tr}\{\mathbf{A}\}$ denoting the trace of the matrix $\mathbf{A}$. On the other hand, the zero-frequency shot
noise, $S = 2 \int_{-\infty}^0 \mathrm{d}t \, (\langle \hat{I}(t)\hat{I}(0) + \hat{I}(0)\hat{I}(t)\rangle - 2\langle \hat{I}\rangle^2)$, is given by

$$S = \frac{e^2}{\hbar} \mathrm{Tr}\{\mathbf{W^{II}P} + \mathbf{W^I \tilde{P} W^I P}\}, \tag{5}$$

where $\mathbf{\tilde{P}}$ is determined from the equation $\mathbf{W\tilde{P} = Q}$, with $Q_{\chi'\chi} = (P_{\chi'} - \delta_{\chi'\chi})(1 - \delta_{\chi'\chi_0})$.

Knowing the current I and the zero-frequency shot noise S, one can determine the Fano
factor F: $F = S/(2e|I|)$. The Fano factor describes the deviation of S from the Poissonian
shot noise given by $S_{\mathrm{p}} = 2e|I|$.

4. Results and discussion

In this section we present numerical and analytical results on the current I, TMR, and Fano
factor F for a two-level quantum dot weakly coupled to the leads. The TMR effect is
phenomenologically defined as [13, 18]

$$\mathrm{TMR} = \frac{I_{\mathrm{P}} - I_{\mathrm{AP}}}{I_{\mathrm{AP}}}, \tag{6}$$

where I_{P} (I_{AP}) is the current flowing through the system when magnetic moments of the leads
are aligned in parallel (antiparallel).

In our considerations we will distinguish between quantum dots coupled symmetrically
and asymmetrically to the leads. The asymmetry may be introduced in various ways—
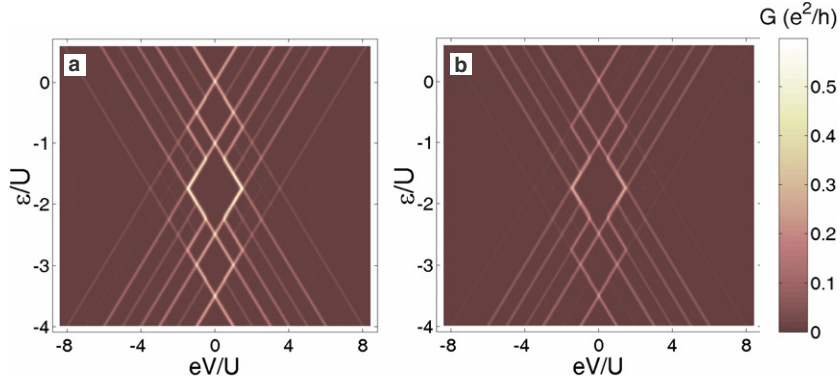for example by attaching the quantum dot to leads with different spin polarizations (e.g.,

Figure 2. The differential conductance $G = \mathrm{d}I/\mathrm{d}V$ as a function of the bias voltage and level position in the parallel (a) and antiparallel (b) magnetic configurations for the parameters $k_\mathrm{B}T = \Gamma$, $\delta\varepsilon = 25\Gamma$, $U = 50\Gamma$, $\Delta = 0$, $p_\mathrm{L} = p_\mathrm{R} \equiv p = 0.7$, and $\Gamma_{rj} \equiv \Gamma/2$ ($r = \mathrm{L}, \mathrm{R}$, $j = 1, 2$).

to one half-metallic and one nonmagnetic lead). On the other hand, if the leads have the same spin polarizations, their coupling to the dot levels may be different. In the following we first consider the case of quantum dots symmetrically coupled to the leads and then we shall proceed to analyse transport through quantum dots asymmetrically coupled to the leads. In order to simplify the following discussion of numerical and analytical results, we set $U_1 = U_2 = U' \equiv U$.

4.1. Quantum dots symmetrically coupled to ferromagnetic leads

In figure 2 we show the differential conductance as a function of the bias voltage V and level position ε. Experimentally, the position of the dot level can be tuned by a gate voltage, therefore figure 2 effectively shows the bias and gate voltage dependence of the differential conductance. The upper part (figure 2(a)) corresponds to the parallel magnetic configuration, whereas the lower part (figure 2(b)) shows the conductance in the antiparallel configuration of the system. Both parts are plotted on the same scale, which facilitates the comparison. First of all, one can note that the conductance in antiparallel configuration is smaller than that in the parallel one. This is due to the spin asymmetry in tunnelling processes, which leads to a partial suppression of the conductance when the leads' magnetizations are antiparallel. The majority (minority) electrons of the source electrode tunnel then to the minority (majority) electron band of the drain electrode, leading effectively to a conductance smaller than that in the parallel configuration. If the spin asymmetry in the density of states increases (the spin polarization of the leads increases), the difference in conductance between these two magnetic configurations becomes larger, which leads to an increase in TMR.

Another feature visible in figure 2 is the diamond-like structure of the differential conductance, which is associated with discrete charging of the quantum dot. The diamonds around $V = 0$ correspond to the Coulomb blockade regions. When lowering the position of the dot levels, the charge of the dot changes successively. More precisely, the dot is empty for $\varepsilon \gtrsim 0$, occupied by one electron for $0 \gtrsim \varepsilon \gtrsim -U$, doubly occupied for $-U \gtrsim \varepsilon \gtrsim -(2U + \delta\varepsilon)$, occupied by three electrons for $-(2U + \delta\varepsilon) \gtrsim \varepsilon \gtrsim -(3U + \delta\varepsilon)$, and the two orbital levels of the dot are fully occupied for $-(3U + \delta\varepsilon) \gtrsim \varepsilon$. In all these transport regions the dot is in a well-defined charge state, and the sequential tunnelling is exponentially suppressed [5, 9]. If the bias voltage is increased above a certain threshold voltage, the current
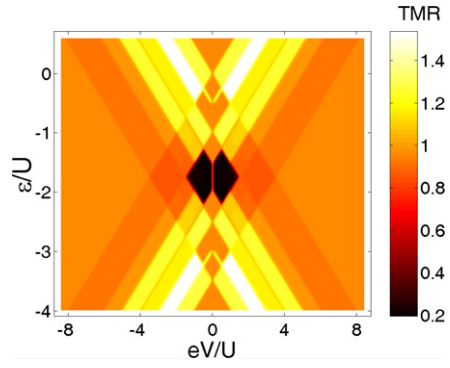
Figure 3. The tunnel magnetoresistance as a function of the bias voltage and level position for the same parameters as in figure 2.

starts to flow due to first-order tunnelling processes. When the charging energy of the dot is much larger than the thermal energy, one observes then a well-resolved step in the current as a function of the bias voltage. In the density plots shown in figure 2, this can be seen in the form of lines that clearly separate the Coulomb blockade regions from transport regions associated with consecutive charge states taking part in transport. When the bias voltage increases further, additional steps (and consequently lines in figure 2) arise at voltages where new states becomes active in transport.

Figure 3 presents the corresponding TMR as a function of the bias and gate voltages. By comparison with figure 2, one can easily identify the regions of Coulomb blockade. First of all, it is worth noting that, depending on the transport region, the TMR takes several well-defined values ranging roughly from 0.2 to 1.6; see figure 3. Such behaviour of TMR is significantly different from that for a single-level quantum dot, where TMR in the sequential tunnelling regime acquires only two values [18]. As follows from figure 3, the TMR in the linear response regime is independent of the gate voltage. More precisely, it is given by $p^2/(1 - p^2)$, which is exactly equal to a half of the TMR calculated within the Julliere model [13]. We recall that the Julliere value of TMR, $TMR_0 = 2p^2/(1 - p^2)$, is characteristic of a single-barrier planar tunnel junction. In the case of double-barrier planar junctions with ferromagnetic leads, the TMR in the sequential transport regime is equal to half of the Julliere value. This applies also to sequential transport through quantum dots coupled to ferromagnetic leads. However, one should bear in mind that transport in the Coulomb blockade regime is dominated by higher-order tunnelling, which can considerably modify the corresponding TMR. For instance, it was shown recently for single-level quantum dots that the TMR in the cotunnelling regime exhibits a strong dependence on the number of electrons on the dot, and for empty or fully occupied dots it reaches the Julliere value [18].

Figure 3 also shows that, when increasing the bias voltage V and keeping constant position of the dot levels, the TMR acquires some specific and well-defined values in different transport regions. To analyse this behaviour in more detail, we show in figures 4(a) and 5(a) the bias voltage dependence of the current and TMR for the case when the dot level is above ($\varepsilon = U/2$) and below ($\varepsilon = -7U/5$) the Fermi level of the leads at equilibrium. As one can see, the current in both magnetic configurations and the associated TMR exhibit characteristic plateaus which correspond to different transport regions. When assuming the zero-temperature limit, one can derive approximate formulae describing transport in each region. However, the analytical solution in a general case is rather complicated due to the 16 different eigenstates involved.
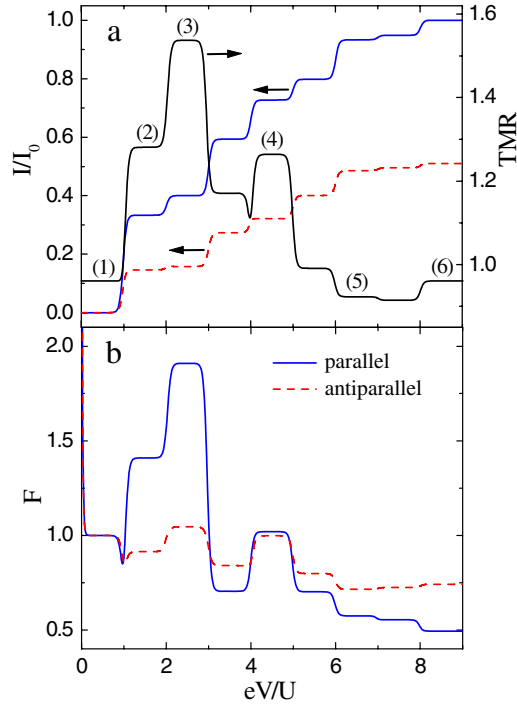
Figure 4. The current (a) in units of $I_0 = e\Gamma/\hbar$ and Fano factor (b) in the parallel (solid line) and antiparallel (dashed line) configurations as well as tunnel magnetoresistance (a) as a function of the bias voltage for $\varepsilon = U/2$. The other parameters are the same as in figure 2.

Therefore, in the following we only present the analytical results for the transport regions, where the corresponding formulae are relatively simple and transparent. These transport regions are marked in figures 4(a) and 5(a) by consecutive numbers. An exemplary analytical calculation of the current in parallel configuration for plateau (3) is described in the appendix.

The analytical expressions for the current $I_{P(AP)}$ and TMR are listed in table 2. First of all, the current depends on the spin polarization of the leads effectively only in the antiparallel configuration, while in the parallel configuration it is independent of p. Such a behaviour is a consequence of the left–right symmetry for each spin channel in the parallel configuration, and equal occupation of the charge states active in transport. This leads to the independence of the average charge and spin of the dot on the polarization factor p, which in turn leads to the charge current being independent of p. This is not the case in the antiparallel configuration, where the symmetry is absent and the current does depend on the spin polarization of the leads. The associated TMR disappears for $p = 0$ and diverges as $p \to 1$ (this is because $I_{AP} \to 0$ for $p \to 1$). For a finite spin polarization p, one finds a considerable enhancement of TMR in regions (2), (3), and (4) as compared to the other transport regions. The maximum TMR occurs in region (3) and is given by $4/5 \times \text{TMR}_0$. This enhancement can be accounted for by realizing that in this transport region all the one-particle states take part in transport, leading to an enhancement of the spin accumulation in the antiparallel configuration. The doubly occupied states do not take part in transport due to the Coulomb energy. In the antiparallel configuration, spin-down electrons of the source electrode can tunnel relatively easily to the dot, where, however, they have to spend a longer time before tunnelling further to the drain electrode.
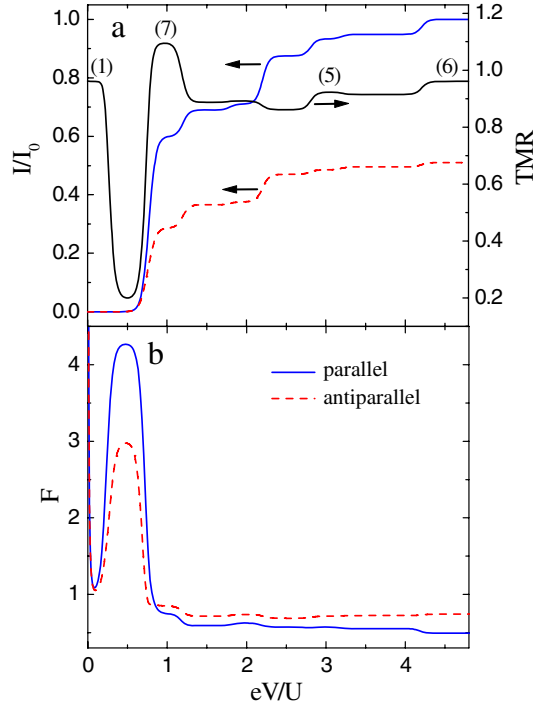
Figure 5. The bias dependence of the current (a), the Fano factor (b) in both magnetic configurations and the TMR (a) calculated for $\varepsilon = -7U/5$. The other parameters are the same as in figure 4. Current is plotted in units of $I_0 = e\Gamma/\hbar$.

Consequently, the current is mainly determined by the tunnelling probability through the barrier between the dot and the drain electrode. This means that a new channel for tunnelling, which becomes active when going from region (2) to region (3), has no significant influence on the current, as is clearly visible in figure 4(a). In turn, in the parallel configuration this new transport channel contributes to the current, increasing this way the difference between the parallel and antiparallel configurations (and consequently the associated TMR).

Although the current flowing through the system in the parallel configuration is independent of the spin polarization in transport regions marked by the numbers, we note that I_P slightly depends on p in the other regions. This is mainly due to the fact that in these regions the occupations of the many-body dot states being active in transport are not equal, leading to a small spin accumulation even in the parallel configuration. For example, in region (2) there are three states taking part in transport, with the occupation probabilities equal to $1/3$; in region (4) there are 11 states (one empty, four single-particle and six two-particle states), all equally occupied with the probability $1/11$, etc. In these regions, the charge current does not depend on spin polarization. However, there are also regions where the occupation probabilities depend on the spin polarization of the leads, such as for example the region between (3) and (4). In this region ten dot states participate in transport (the same as in region (4) except for the state with doubly occupied second level). We find that in this region the dot states do not take part in transport on an equal footing, which leads to small spin accumulation. This is a consequence of the interplay between the energy structure of the dot and ferromagnetism of the electrodes. The spin accumulation disappears when transport goes through single-particle

9

Table 2. Analytical expressions approximating the current I_P (I_{AP}), the Fano factor F_P (F_{AP}) in the parallel (antiparallel) magnetic configuration, and the TMR in different transport regimes corresponding to plateaus shown in figures 4 and 5 for $p_L = p_R \equiv p$. The current is expressed in units of $I_0 = e\Gamma/\hbar$. In the Coulomb blockade regime, where the current is suppressed, the TMR was determined from the linear conductance.

Plateau	I_P	I_{AP}	TMR	F_P	F_{AP}
(1)	0	0	$\dfrac{p^2}{1-p^2}$	1	1
(2)	$\dfrac{1}{3}$	$\dfrac{1-p^2}{3+p^2}$	$\dfrac{4p^2}{3-3p^2}$	$\dfrac{5+3p^2}{9(1-p^2)}$	$\dfrac{(5-p^2)(1+3p^2)}{(3+p^2)^2}$
(3)	$\dfrac{2}{5}$	$\dfrac{2(1-p^2)}{5+3p^2}$	$\dfrac{8p^2}{5-5p^2}$	$\dfrac{17+15p^2}{25(1-p^2)}$	$\dfrac{17+(62-15p^2)p^2}{(5+3p^2)^2}$
(4)	$\dfrac{8}{11}$	$\dfrac{8(1-p^2)}{11+(2+3p^2)p^2}$	$\dfrac{(13+3p^2)p^2}{11(1-p^2)}$	$\approx \dfrac{0.55}{1-p^2}$	$\approx \dfrac{0.55+(2-p^2)(0.6+p^2)p^2}{(1+0.2p^2+0.3p^4)^2}$
(5)	$\dfrac{14}{15}$	$\dfrac{2(1-p^2)(7+p^2)}{(5-p^2)(3+p^2)}$	$\dfrac{8(13+p^2)p^2}{15(1-p^2)(7+p^2)}$	$\approx \dfrac{0.5-0.45p^2}{1-p^2}$	$\approx \dfrac{5+7p^2}{10+4p^2}$
(6)	1	$1-p^2$	$\dfrac{p^2}{1-p^2}$	$\dfrac{123+5p}{256}$	$\dfrac{123+(5+133p-5p^2)p}{256}$
(7)	$\dfrac{3}{5}$	$\dfrac{(1-p^2)(3+p^2)}{5+(2+p^2)p^2}$	$\dfrac{8(2+p^2)p^2}{5(1-p^2)(3+p^2)}$	$\approx \dfrac{0.47-0.2p^2}{1-p^2}$	$\approx \dfrac{5(7+19p^2+26p^4)}{(3+p^2)(5+2p^2+p^4)^2}$

states. This simply follows from the same spin asymmetry of tunnelling through the left and right barriers. If we have transport through doubly occupied states with Coulomb interaction, the situation becomes more complex. The Coulomb interaction in some situations may suppress this symmetry, leading to spin accumulation. We note that similar spin accumulation for the parallel magnetic configuration in symmetric junctions was also observed in different systems; see e.g. [39].

A new and interesting behaviour of TMR may be observed in the blockade region, where the dot is doubly occupied; see figures 3 and 5(a). Contrary to the case of a single-level quantum dot, where sequential TMR is constant in the whole blockade regime, the TMR displays now a strong dependence on the bias voltage. Once the voltage is increased to around $eV \approx U/2$, the TMR drops rapidly from $1/2 \times \text{TMR}_0$ to about $1/10 \times \text{TMR}_0$ and then, on further increasing the bias voltage, the TMR increases to the value corresponding to the plateau (7); see table 2. This leads to a deep minimum in the TMR clearly visible in figure 5(a), which can also be seen in figure 3 as the two black areas in the middle of the figure.

We have also calculated the Fano factor F_P and F_{AP} in the parallel and antiparallel magnetic configurations, respectively. The zero-frequency shot noise can then be found from the knowledge of the current I and the Fano factor F. The Fano factor for the two situations discussed above, and corresponding to figures 4(a) and 5(a), is shown in figures 4(b) and 5(b) for both magnetic configurations. Similarly to the case of current and TMR, the Fano factor acquires roughly constant values, different in different transport regions. The relevant analytical formulae, obtained with the same assumptions as before, are given in table 2. Due to the spin asymmetry in the coupling of the dot to external leads, the bias dependence of the Fano factor is significantly different from that in the corresponding nonmagnetic situations [21]. For both magnetic configurations of the system, the Fano factor depends on the polarization factor p (differently in the two configurations, in general), except for the case of empty dot where the exponentially suppressed transport gives rise to a Poissonian Fano factor $F_P = F_{AP} = 1$. In addition, if $|eV| \ll k_B T$, the Fano factor becomes divergent due to the thermal noise, which dominates in this transport regime; in the case of $V = 0$, the noise is given by $S = 4k_B T G^{\text{lin}}$, with G^{lin} being the linear conductance, leading to a divergency of the Fano factor (finite S

for $I = 0$) [40, 41]. Furthermore, in some transport regions we find $F_P > F_{AP}$, while in the other ones $F_P < F_{AP}$. As one can see from the expressions listed in table 2, the ratio F_P/F_{AP} depends on the spin polarization of the leads p. For example, in region (2) $F_P > F_{AP}$ only if $p \gtrsim 0.37$. Furthermore, if the leads are half-metallic, the Fano factor in the parallel configuration diverges as $p \to 1$, except for regions (1) and (6), where $F_P = 1$ and $1/2$, respectively. On the other hand, in the antiparallel configuration the Fano factor tends to unity for $p \to 1$, except for the Coulomb blockade regime with two electrons trapped in the dot, where we find super-Poissonian shot noise, $F_{AP} \approx 3$; see figure 5(b).

The super-Poissonian shot noise in the Coulomb blockade regime with two electrons trapped in the dot, shown in figure 5(b), can be accounted for as follows. In the ground state the dot is occupied by two electrons on the first level (of lower energy). Assume the voltage corresponding to the maximum of the peak in the Fano factor, $eV/U \approx 0.5$. The system is still in the blockade regime (compare figure 5(a)), where the current is exponentially suppressed. A nonzero small current can flow due to thermal excitations. There is an exponentially small probability that one electron leaves the dot and the other one jumps to the dot either to the same (first) or to the second energy level (of higher energy). If it tunnels to the second energy level, then transport through this level is allowed and electron can easily leave the dot, while another one can jump to the same level or to the level of lower energy. If it tunnels to the same level, further tunnelling processes are allowed. If it tunnels to the low-energy (first) level, the system is blocked again. This leads to large fluctuations in the current, and consequently to super-Poissonian shot noise shown in figure 5(b). This behaviour does not result from magnetism of the electrodes and persists even in the case of nonmagnetic leads, where the Fano factor is approximately $F \approx 3$. The effect is only quantitatively modified by ferromagnetism of the electrodes—the magnitude of the super-Poissonian shot noise is different in parallel and antiparallel configurations, as shown in figure 5(b).

On the other hand, the increase of the Fano factor in the parallel configuration, observed when $p \to 1$, is due to the enhanced spin asymmetry in transport processes through the dot [16, 42]. Consider for instance region (2) in figure 4(b). Spin-up electrons then tunnel relatively easily into and out of the dot. However, when a spin-down electron appears on the dot, it blocks transport for relatively long time, leading to large fluctuations in the current. These fluctuations increase when $p \to 1$, giving rise to a super-Poissonian Fano factor, which is characterized by a divergent component $F_P \sim (1 - p^2)^{-1}$. In turn, such fluctuations are absent in the antiparallel configuration and the shot noise is Poissonian, $F_{AP} \sim 1$ for $p \to 1$.

4.2. Quantum dots asymmetrically coupled to the leads

In the previous subsections we have analysed transport through quantum dots coupled symmetrically to ferromagnetic leads (equal spin polarizations of the leads and equal coupling parameters). In that case transport characteristics were symmetric with respect to the bias reversal. However, when the dot is coupled asymmetrically to the leads, the I–V curves are no longer symmetric with respect to the bias reversal, leading to further interesting effects. In the following, we discuss transport properties of quantum dots asymmetrically coupled to the leads and consider two special cases. The first case concerns the quantum dot coupled to one nonmagnetic and one half-metallic lead ($p_L \equiv p$, $p_R = 0$ and $\Gamma_{1r} = \Gamma_{2r'}$), whereas in the second case the dot is coupled to the leads with equal spin polarizations but with unequal coupling strengths ($p_L = p_R \equiv p$ and $\Gamma_{1r} \neq \Gamma_{2r'}$). It has been shown recently that transport characteristics of a single-level quantum dots coupled to one half-metallic and one nonmagnetic lead display a diode-like behaviour [15, 16, 43]. On the other hand, in the nonmagnetic limit of the second case a negative differential conductance has been found [21].
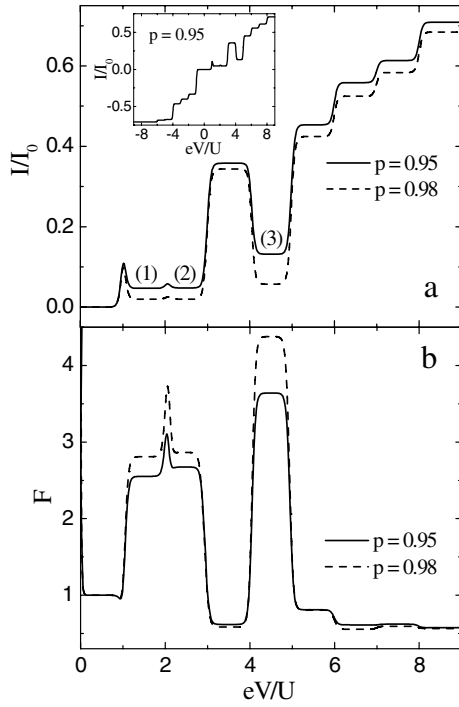
Figure 6. The current (a) in units of $I_0 = e\Gamma/\hbar$ and Fano factor (b) as a function of the bias voltage for $p_L \equiv p = 0.95, 0.98$, $p_R = 0$, while the other parameters are the same as in figure 2. The inset in part (a) shows the current in the whole range of the bias voltage.

4.2.1. Unequal spin polarizations of the leads. When one of the leads is half-metallic ($p = 1$) and the other one is nonmagnetic ($p = 0$), the transport characteristics become asymmetric with respect to the bias reversal. Furthermore, the current can be suppressed in certain bias regions, and this suppression is accompanied by the occurrence of NDC. This basically happens when the electrons residing in the dot have spin opposite to that of electrons in the half-metallic drain electrode. In figure 6 we show the current and Fano factor for a quantum dot coupled to half-metallic (left) and nonmagnetic (right) lead as a function of the bias voltage. For the parameters assumed, the current is suppressed in certain ranges of positive bias voltage. As follows from figure 6, there are three blockade regions. To facilitate the further discussion, we label these blockade regions with numbers, as indicated in figure 6(a). On the other hand, for negative bias voltage, the current changes monotonically with the transport voltage, as one can see in the inset of figure 6(a).

In the blockade region (1), $1 \lesssim eV/U \lesssim 2$, the dot is in the state $|\downarrow\rangle|0\rangle$ and the spin-down electron residing in the dot has no possibility to tunnel further to the left lead, which leads to suppression of the current. The blockade region (2), $2 \lesssim eV/U \lesssim 3$, is associated with the occupation of the states $|\downarrow\rangle|0\rangle$ and $|0\rangle|\downarrow\rangle$. The current is then prohibited due to the full occupation of the single-particle spin-down states. When increasing the bias voltage further, $3 \lesssim eV/U \lesssim 4$, the blockade of the current becomes suppressed (see the plateau between regions (2) and (3) in figure 6(a)), which is due to a finite occupation of state $|\uparrow\downarrow\rangle|0\rangle$. Although tunnelling of spin-down electrons is then blocked, the current is still carried by spin-up electrons. In turn, the blockade region (3) occurs for $4 \lesssim eV/U \lesssim 5$, where the dot is in the triplet state $|\downarrow\rangle|\downarrow\rangle$ and tunnelling is also suppressed. Thus, the current is blocked when the

12

total dot spin S_z is either $S_z = -1/2$ or -1, i.e., the spin of electrons on the dot is opposite to that of electrons in the half-metallic lead. There is no suppression of the current for negative voltage. This is because the electrons residing in the dot can always tunnel to the nonmagnetic drain electrode.

The current blockade in regions (1)–(3) in figure 6(a) for positive bias is not due to the charging effects as in the Coulomb blockade regime, but due to a particular occupation of the dot spin state. Such blockade is frequently referred to as the Pauli spin blockade, and it has already been found in single-dot and double-dot systems [44–46]. Here, we show that the Pauli spin blockade can occur in single two-level quantum dots, provided they are coupled to half-metallic lead(s). It is further worth noting that the blockade of the current in figure 6(a) is not complete: there is a small leakage current inside each blockade region, which results from the fact that the assumed spin polarization of the half-metallic lead is not exactly equal to unity. When the spin polarization is increased, the current in the blockade regions decreases (compare the curves for $p = 0.95$ and 0.98).

The spin blockade of charge current leads to the super-Poissonian shot noise, i.e., the corresponding Fano factor is larger than unity. On the other hand, the Fano factor outside the spin blockade regions is sub-Poissonian (smaller than unity), as shown in figure 6(b). The enhancement of the shot noise in the Pauli blockade regions is a consequence of large spin asymmetry in the tunnelling processes. The occurrence of a spin-down electron on the dot prevents further tunnelling processes for a longer time, while spin-up electrons on the dot can escape much more quickly, allowing further tunnelling processes. This gives rise to large current fluctuations, and consequently also to Fano factors much larger than unity.

Assuming the zero-temperature limit, one can find approximate expressions for the current (in units of $I_0 = e\Gamma/\hbar$) in the spin blockade regions

$$I^{(1)} = \frac{1 - p^2}{3 - p^2}, \tag{7}$$

for the first (1),

$$I^{(2)} = \frac{2(1 - p^2)}{5 - p^2}, \tag{8}$$

second (2), and

$$I^{(3)} = \frac{2(1 - p^2)(2 - p^2)}{11 - 8p^2 + p^4}, \tag{9}$$

for the third blockade region, (3); see figure 6(a). The above formulae show that the current vanishes when $p \to 1$. This is due to the total blockade of charge transport by spin-down electrons in the dot. This can be also concluded from the respective occupation probabilities, which are given by $P_{|\downarrow\rangle|0\rangle}^{(1)} = (1 + p)/(3 - p^2)$ for the first blockade regime, $P_{|\downarrow\rangle|0\rangle}^{(2)} = P_{|0\rangle|\downarrow\rangle}^{(2)} = (1 + p)/(5 - p^2)$ for the second one, and $P_{|\downarrow\rangle|\downarrow\rangle}^{(3)} = (1 + p)^2/(11 - 8p^2 + p^4)$ for the third blockade region. It is clearly evident from these formulae that the corresponding occupations approach unity for $p \to 1$, leading to the full spin blockade. It is also interesting to note that in region (3) one observes formation of a pure triplet state.

With the same approximations as above, one can find the corresponding formulae for the Fano factor in the spin blockade regions

$$F^{(1)} = \frac{(1 + p^2)(5 + p^2)}{(3 - p^2)^2}, \tag{10}$$

for the region (1), and

$$F^{(2)} = \frac{17 + 30p^2 + p^4}{(5 - p^2)^2}, \tag{11}$$

13

for region (2). From the above expressions it follows that $F^{(1)} = 5/9$ and $F^{(2)} = 17/25$ for $p = 0$, i.e., the shot noise is sub-Poissonian, However, for $p \to 1$ the noise becomes super-Poissonian, $F^{(1)} = 3$ and $F^{(2)} = 51/16$. In the third spin blockade regime, the analytical formula for the Fano factor $F^{(3)}$ is too cumbersome to be presented here. It is, however, worth noting that $F^{(3)} \approx 0.55$ for $p = 0$, while $F^{(3)} = 5$ for $p \to 1$. In addition, from the analytical expressions for the Fano factor one can easily estimate the value of spin polarization p at which the shot noise becomes super-Poissonian. This gives $F^{(1)} > 1$ for $p > 1/\sqrt{3}$, and $F^{(2)} > 1$ for $p > 1/\sqrt{5}$.

4.2.2. Unequal coupling of the dot levels to the leads. It has been shown recently that a negative differential conductance (NDC) can occur in transport characteristics of two-level quantum dots, when the two orbital levels are coupled to nonmagnetic leads with different coupling strengths [21]. In the following, we consider the dot coupled to ferromagnetic leads of equal spin polarizations, but with unequal coupling strengths. For one bias polarization we find narrow bias regions where NDC occurs, followed by the regions where the current is partly suppressed. The suppression of current is accompanied by a super-Poissonian shot noise and may lead to negative TMR, as shown in figure 7, where the current and Fano factor in the parallel and antiparallel magnetic configurations as well as the corresponding TMR are plotted as a function of the bias voltage. As one can see, NDC and the associated regions where charge current is partly suppressed occur in both magnetic configurations of the system. The suppression regions are marked with (1), (2) and (3), see figure 7(a), and occur for $2 \lesssim eV/U \lesssim 3$, $4 \lesssim eV/U \lesssim 5$, and $6 \lesssim eV/U \lesssim 7$, respectively.

In the blockade region (1), the dot can be occupied by at most one electron. The blocking mechanism is associated with an increased occupation of the second orbital level and decreased occupation of the first level. Since the coupling of the second level to the left lead (drain for electrons at positive bias) is the weakest coupling in the system (the others are assumed to be equal), the average occupation of this level is larger than the occupation of the first level. Thus, an electron that has tunnelled from the right lead to the second level spends a long time in the dot before it tunnels further to the right lead and, consequently, blocks transport through the first level. In other words, the onset of electron tunnelling to the second level of the dot leads to the suppression of current (NDC and the associated suppression region). In turn, no NDC and current suppression takes place for negative bias voltage, as now an electron that has tunnelled to the second level can easily tunnel further to the drain (right) electrode. From the above discussion it follows that the suppression of current for positive bias voltage occurs in those transport regions, where the occupation of the second level is larger than that of the first dot level, and the rate for tunnelling between the second level and the drain electrode is smaller than that for the source electrode. The same scenario also holds for the next two blockade regions. In region (2) it is the increased occupation of the state $|0\rangle|\uparrow\downarrow\rangle$ which is responsible for the blockade, whereas in region (3) transport is mainly mediated through the states $|0\rangle|\uparrow\downarrow\rangle$, $|\uparrow\rangle|\uparrow\downarrow\rangle$, and $|\downarrow\rangle|\uparrow\downarrow\rangle$. If the second level is completely decoupled from the left lead, transport in region (3) is still mediated through the single-particle states of the first orbital level. This is why there is only a weak suppression of the current in this blockade region, as compared to the first and second blockade regions, where the current can be fully suppressed.

In the zero-temperature limit one can derive some analytical formulae for the current, TMR and Fano factor in all three blockade regions. First of all, it is interesting to note that NDC in regime (1) occurs when $x < 1/3$ and $x < (1 + p^2)/(3 + p^2)$ for the parallel and antiparallel configurations, respectively, with $x = \Gamma_{L2}/\Gamma$. The parameter x describes the asymmetry between the coupling of the second dot level to the left lead and the other couplings, $\Gamma_{L1} = \Gamma_{R1} = \Gamma_{R2} = \Gamma/2$. Thus, for $x \to 0$ the second dot level is completely
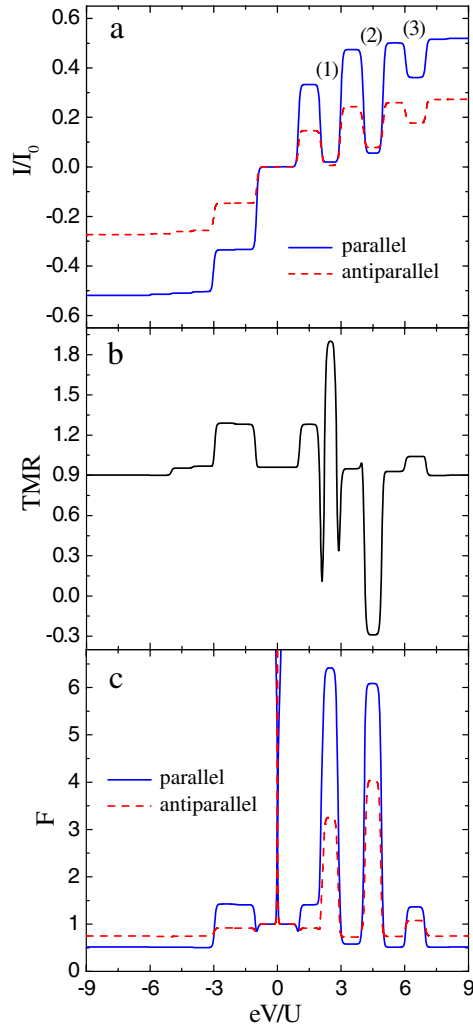
Figure 7. The current (a) in units of $I_0 = e\Gamma/\hbar$ and the Fano factor (b) in the parallel (solid line) and antiparallel (dashed line) configurations, and the resulting TMR (c) as a function of the bias voltage for $\varepsilon = 25\Gamma$ and $\Gamma_{L1} = \Gamma_{R1} = 50\Gamma_{L2} = \Gamma_{R2} \equiv \Gamma/2$. The other parameters are the same as in figure 2.

decoupled from the left lead, whereas for $x = 1/2$ one recovers the symmetric case. The current (in units of I_0) in both magnetic configurations is given by $I_P^{(1)} = 2x/(1 + 3x)$ and $I_{AP}^{(1)} = 2(1 - p^2)x/[1 + 3x + (1 + x)p^2]$, whereas the TMR is

$$\text{TMR}^{(1)} = \frac{2p^2}{1 - p^2} \frac{1 + 2x}{1 + 3x}. \tag{12}$$

It is worth noting that the current tends to zero for $x \to 0$, whereas the TMR approaches TMR_0. The formulae for the Fano factor are too complex to be written here explicitly. However, we find that for $x \to 0$, $F_P^{(1)} = (3 + p^2)/(1 - p^2)$ and $F_{AP}^{(1)} = (3 + 10p^2 - p^4)/(1 + p^2)^2$ for the parallel and antiparallel configurations, respectively, which yields super-Poissonian shot noise, irrespective of the spin polarization of the leads.

15

It is also possible to derive analytical formulae for the current, TMR, and the conditions for NDC in the other blockade regions. However, they are not simple and would make the discussion somehow obscure. Therefore, we will only consider two limiting situations, i.e., the symmetric case and the case of $x \to 0$, where the formulae become relatively simple. When the couplings are symmetric, the blockade is lifted and the current, TMR and Fano factor in the blockade regimes are given by the expressions corresponding to the third, fourth and fifth plateaus, as listed in table 2. When the second level is decoupled from the left lead ($x \to 0$), current in the second blockade regime tends to zero, while the TMR becomes negative and is given by $\mathrm{TMR}^{(2)} = -4p^2/(3 + p^2)$; see figure 7(b).

To understand the physical mechanism leading to the negative sign of TMR let us assume a small value of x and that the dot is in the blocked state with two electrons on the second level. When a spin-up electron tunnels from the dot to the left lead (this tunnelling probability is higher than for spin-down electrons), the system becomes unblocked, and the next blockade takes place when a spin-up electron from the right lead tunnels to the dot. This tunnelling probability is larger in the parallel configuration than in the antiparallel (in the former case it involves spin majority electrons while in the latter case spin minority ones). Thus, the blockade is more effective in the parallel configuration than in the antiparallel one, leading to negative TMR for small values of x, as shown in figure 7(b). For the parameters assumed to calculate figure 7, the TMR changes sign when $x \lesssim 0.023$. For the Fano factor in the limit of $x \to 0$ we find $F_{\mathrm{AP}}^{(2)} > F_{\mathrm{P}}^{(2)}$ for $p < 1$. However, if $p \to 1$ the Fano factor is divergent in both magnetic configurations of the system. Furthermore, in the limit of $x \to 0$, the shot noise becomes super-Poissonian, irrespective of the magnetic configuration of the system and spin polarization p. For $p = 0$, the Fano factor is minimum and is given by $F_{\mathrm{P}}^{(2)} = F_{\mathrm{AP}}^{(2)} \approx 4.9$.

Contrary to the first two blockade regions, the current in the third blockade region is finite for $x \to 0$. This is due to the fact that although tunnelling through the second level is suppressed, current can be still mediated by single-particle states of the first level. In the zero-temperature limit the current in the parallel and antiparallel configurations is given by (in units of I_0) $I_{\mathrm{P}}^{(3)} = 1/3$ and $I_{\mathrm{AP}}^{(3)} = (1 - p^2)/(3 + p^2)$, respectively. This yields the tunnel magnetoresistance $\mathrm{TMR}^{(3)} = 4p^2/(3 - 3p^2) = 2/3 \times \mathrm{TMR}_0$, which is characteristic for the transport regime where single-particle states take part in transport; see the formulae for plateau (2) in table 2. The Fano factor in the case of negligible coupling $\Gamma_{\mathrm{L}2}$ in both magnetic configurations is $F_{\mathrm{P}}^{(3)} = (5 + 3p^2)/(9 - 9p^2)$ and $F_{\mathrm{AP}}^{(3)} = (5 - p^2)(1 + 3p^2)/(3 + p^2)^2$, respectively. This implies that $F_{\mathrm{AP}}^{(3)} \leqslant 1$ for all p, while $F_{\mathrm{P}}^{(3)}$ becomes larger than unity for $p > 1/\sqrt{3}$.

As follows from the above discussion, a distinctively different transport behaviour of the system can be found in each blockade region, when the coupling of the second level to the left lead is negligible. This is especially visible in TMR which in the first blockade region approaches the Julliere value, and in the second blockade changes sign and becomes negative, while in the third blockade region it is given by 2/3 of the Julliere value. Furthermore, in the two first blockade regions we find a full suppression of the current for $x \to 0$, accompanied by a super-Poissonian shot noise. It is also worth noting that the origin of the blockade is now different from that discussed previously (Pauli spin blockade), although some qualitative features of the blockade are very similar.

4.3. Effect of external magnetic field

So far we have assumed that the dot levels are spin degenerate. However, in a strong magnetic field the Zeeman energy can be large enough (of the order of Γ or larger) to influence the transport characteristics significantly [34]. The impact of an external magnetic field on
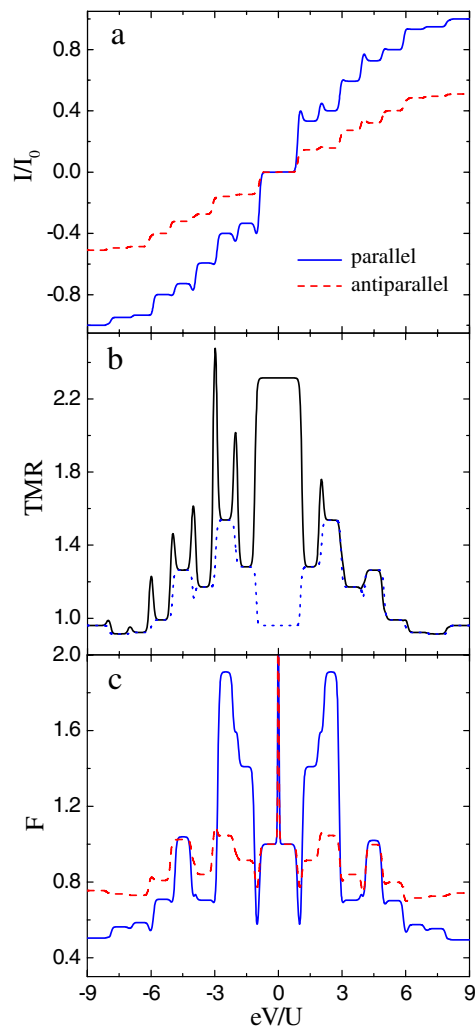
Figure 8. The current (a) in units of $I_0 = e\Gamma/\hbar$ and Fano factor (c) in the parallel (solid line) and antiparallel (dashed line) configurations as well as the TMR (b) as a function of the bias voltage in the presence of external magnetic field, $\Delta = 5\Gamma$. The other parameters are the same as in figure 2. For comparison we also show the TMR in the case of $\Delta = 0$; see the dotted (blue) line in part (b).

transport properties is the most visible in the case of symmetric couplings; therefore only this situation is discussed in the following.

The bias dependence of the current and Fano factor in both magnetic configurations and the corresponding TMR are shown in figure 8 for the symmetric system and in the presence of external magnetic field. Because of a finite Zeeman splitting of the dot levels, there is now an asymmetry of transport characteristics with respect to the bias reversal. Moreover, NDC occurs now for both positive and negative bias voltages, irrespective of magnetic configuration of the system, as clearly visible in figure 8(a). The NDC is, however, more pronounced in the parallel configuration than in the antiparallel one.

The TMR is displayed in figure 8(b), where, for comparison, the TMR in the absence of magnetic field is also shown. If the energy levels are split due to the Zeeman energy, the TMR

17

exhibits characteristic peaks which occur at voltages corresponding to the Coulomb steps in the I–V curves. These peaks are more visible for negative bias voltage. In addition, a high plateau evolves in the low bias range due to the splitting of the dot levels. To determine the analytic formula for the TMR in the linear response, we consider the linear conductance, which in the case of $\Delta \gg k_{B}T$ and low temperature can be approximated by $G_{P}^{lin} \sim (1 + p)/2$ and $G_{AP}^{lin} \sim (1 - p^2)/2$, for the parallel and antiparallel configurations, respectively. This yields for the TMR

$$TMR^{lin} = p/(1 - p). \tag{13}$$

It is worth noting that the TMR is now much enhanced as compared to the case of no external magnetic field, where the TMR is given by $p^2/(1 - p^2)$. Moreover, the linear TMR in the presence of magnetic field is even larger than the Julliere value of TMR. The enhancement of TMR is due to the fact that when $\Delta \gg k_{B}T$, the thermally activated sequential transport takes place only through the state $|\uparrow\rangle|0\rangle$ and not through states $|\uparrow\rangle|0\rangle$ and $|\downarrow\rangle|0\rangle$ as in the case of $\Delta = 0$. This considerably increases the spin asymmetry of the total current in both magnetic configurations, and gives rise to enhanced TMR in the linear response regime. The peak structure of TMR results from the corresponding peaks in current, shown in figure 8(a). More specifically, when the dot levels are spin-split, the two spin contributions to current differ not only in magnitude, but also in positions of the steps (peaks in the corresponding differential conductance). Adding the two contributions leads to characteristics of the current with a pronounced peak structure. This structure is much more visible in the parallel configuration than in the antiparallel one. This simply follows from spin asymmetry—note that for vanishing Zeeman splitting the two contributions to current become equivalent in the antiparallel configuration, but are still significantly different in the parallel one.

The Fano factor in both magnetic configurations is shown in figure 8(c). Contrary to the current and TMR, the behaviour of the Fano factor is only slightly changed as compared to the case of a quantum dot in the absence of magnetic field; see figures 4 and 8(c). This is because Zeeman splitting does not provide a mechanism leading to a qualitative change of the noise— the noise and current are modified in a similar way, so the corresponding Fano factor is only weakly affected by magnetic field.

5. Summary

We have considered spin-polarized transport through a two-level quantum dot coupled to ferromagnetic leads in the sequential tunnelling regime. The cases of symmetric and asymmetric coupling of the dot to external leads have been analysed. For the most characteristic transport regions we have derived approximate analytical formulae for the current and Fano factor in the parallel and antiparallel configurations, as well as for the TMR effect. These formulae may be useful in the interpretation of future experimental data.

Transport properties of quantum dots symmetrically coupled to the leads are shown to be strongly dependent on the bias and gate voltages. First of all, the bias and gate voltage dependence of TMR is then significantly different from that in the case of single-level quantum dots. The TMR can take now several well-defined values, which depend on the parameters of the system. Furthermore, we have shown that the shot noise in the parallel configuration may become super-Poissonian in some transport regions. In the antiparallel configuration the noise is rather sub-Poissonian and the Fano factor becomes equal to unity when the leads become half-metallic.

We have also shown that, for a quantum dot coupled to one half-metallic and one nonmagnetic lead, the current is suppressed in certain bias regions. The suppression of the

current results from the full occupation of the relevant dot spin state. A super-Poissonian shot noise has been found in these blockade regions. On the other hand, in the case when there is an asymmetry between the couplings of the dot levels to external leads, some blockade regions accompanied by NDC have been observed in both magnetic configurations of the system. We found three blockade regions with significantly different behaviour of the TMR effect. In the regions where NDC occurs, the Fano factor is larger than unity and the shot noise is super-Poissonian.

Additionally, the effect of a finite Zeeman splitting of the dot levels was discussed in the case of quantum dot coupled symmetrically to the leads. We have shown that NDC occurs in both magnetic configurations, and for both bias polarizations. Furthermore, the TMR exhibits peaks at voltages corresponding to consecutive Coulomb steps, and a high plateau in the TMR appears in the linear response regime. Unlike the current and TMR, the Fano factor was found to be only slightly affected by an external magnetic field.

The numerical results presented in this paper have been calculated for $U_1 = U_2 = U'$. However, the results for a general case, where the Coulomb integral between two electrons localized on different orbitals is different from the Coulomb integral for two electrons occupying the same orbital, are qualitatively similar and the difference is rather of quantitative nature. More specifically, the lengths of different plateaus on the voltage scale may now be different, which is a consequence of the fact that the charging energy depends now on the distribution of electrons between the two orbitals of the quantum dot. Apart from this, the heights of the plateaus may also be different as compared to the case when all Coulomb integrals are equal.

Acknowledgments

Appendix

In the following we describe the procedure to derive the analytical formulae presented in table 2. As an example, we calculate the current in the parallel configuration for the transport region (3) shown in figure 4. In this region there are five dot states taking part in transport: these are the empty state and all the four single-particle states; see table 1. As the occupations and contribution to the current coming from the other states are suppressed, it is sufficient to consider only the transitions (self-energies) between the above-mentioned five states. In the low-temperature limit we approximate the Fermi–Dirac functions by step functions and get for the full self-energy matrix in the basis defined by these five dot states

$$
\mathbf{W} = \begin{pmatrix}
-2\Gamma & (1+p)\Gamma/2 & (1-p)\Gamma/2 & (1+p)\Gamma/2 & (1-p)\Gamma/2 \\
(1+p)\Gamma/2 & -(1+p)\Gamma/2 & 0 & 0 & 0 \\
(1-p)\Gamma/2 & 0 & (p-1)\Gamma/2 & 0 & 0 \\
(1+p)\Gamma/2 & 0 & 0 & -(1+p)\Gamma/2 & 0 \\
(1-p)\Gamma/2 & 0 & 0 & 0 & (1-p)\Gamma/2
\end{pmatrix}.
$$

By replacing one row of $\mathbf{W}$ with $(\Gamma, \ldots, \Gamma)$, which is due to normalization, one can calculate the occupation probabilities from equation (3). For plateau (3) and parallel configuration one

finds that the probabilities are equal and given by $1/5$, i.e. each of the five states is equally occupied. In a similar way one can determine the elements of the self-energy matrix $\mathbf{W^I}$:

$$\mathbf{W^I} = \begin{pmatrix} 0 & -(1+p)\Gamma/2 & (p-1)\Gamma/2 & -(1+p)\Gamma/2 & (p-1)\Gamma/2 \\ -(1+p)\Gamma/2 & 0 & 0 & 0 & 0 \\ (p-1)\Gamma/2 & 0 & 0 & 0 & 0 \\ -(1+p)\Gamma/2 & 0 & 0 & 0 & 0 \\ (p-1)\Gamma/2 & 0 & 0 & 0 & 0 \end{pmatrix}.$$

It is now possible to calculate the current from equation (4), which gives $I_P = 2e\Gamma/5\hbar$. The other analytical expressions can be determined in the same manner.

References

[1] Wolf S A, Awschalom D D, Buhrman R A, Daughton J M, von Molnar S, Roukes M L, Chtchelka A Y and Treger D M 2001 *Science* **294** 1488
[2] Awschalom D D, Loss D and Samarth N 2002 *Semiconductor Spintronics and Quantum Computation* (Berlin: Springer)
[3] Maekawa S and Shinjo T 2002 *Spin Dependent Transport in Magnetic Nanostructures* (London: Taylor and Francis)
[4] Zutic I, Fabian J and Das Sarma S 2004 *Rev. Mod. Phys.* **76** 323
[5] Kouwenhoven L P, Marcus C M, McEuen P L, Tarucha S, Westervelt R M and Wingreen N S 1997 *Proc. NATO Advanced Study Institute on Mesoscopic Electron Transport (Kluwer Series E345)* ed L L Sohn, L P Kouwenhoven and G Schön
[6] Kouwenhoven L and Marcus C 1998 *Phys. World* **11** (June) 35
[7] Deshmukh M M and Ralph D C 2002 *Phys. Rev. Lett.* **89** 266803
[8] Hanson R, Witkamp B, Vandersypen L M K, Willems van Beveren L H, Elzerman J M and Kouwenhoven L P 2003 *Phys. Rev. Lett.* **91** 196802
[9] Grabert H and Devoret M H 1992 *Single Charge Tunneling: Coulomb Blockade Phenomena in Nanostructures* (*NATO ASI Series B: Physics* vol 294) (New York: Plenum)
[10] Sohn L L, Kouwenhoven L P and Schön G 1997 *Mesoscopic Electron Transport* (Dordrecht: Kluwer)
[11] Likharev K K 1999 Single-electron devices and their applications *Proc. IEEE* **87** 606
[12] Heinzel T 2003 *Mesoscopic Electronics in Solid State Nanostructures* (New York: Wiley–VCH)
[13] Julliere M 1975 *Phys. Lett.* A **54** 225
[14] Barnaś J and Fert A 1998 *Phys. Rev. Lett.* **80** 1058
Takahashi S and Maekawa S 1998 *Phys. Rev. Lett.* **80** 1758
[15] Rudziński W and Barnaś J 2001 *Phys. Rev.* B **64** 085318
[16] Bułka B R 2000 *Phys. Rev.* **62** 1186
[17] König J and Martinek J 2003 *Phys. Rev. Lett.* **90** 166602
[18] Weymann I, König J, Martinek J, Barnaś J and Schön G 2005 *Phys. Rev.* B **72** 115334
[19] Weymann I, Barnaś J, König J, Martinek J and Schön G 2005 *Phys. Rev.* B **72** 113301
[20] Weymann I and Barnaś J 2005 *Eur. Phys. J.* B **46** 289
[21] Thielmann A, Hettler M H, König J and Schön G 2005 *Phys. Rev.* B **71** 045341
[22] Belzig W 2004 *Phys. Rev.* B **71** 161301(R)
[23] Elste F and Timm C 2006 *Phys. Rev.* B **73** 235305
[24] Chye Y, White M E, Johnston-Halperin E, Gerardot B D, Awschalom D D and Petroff P M 2002 *Phys. Rev.* B **66** 201301(R)
[25] Heersche H B, de Groot Z, Folk J A, Kouwenhoven L P, van der Zant H S J, Houck A A, Labaziewicz J and Chuang I L 2006 *Phys. Rev. Lett.* **96** 017205
[26] Zhang L Y, Wang C Y, Wei Y G, Liu X Y and Davidović D 2005 *Phys. Rev.* **72** 155445
[27] Tsukagoshi K, Alphenaar B W and Ago H 1999 *Nature* **401** 572
[28] Zhao B, Mönch I, Vinzelberg H, Mühl T and Schneider C M 2002 *Appl. Phys. Lett.* **80** 3144
Zhao B, Mönch I, Vinzelberg H, Mühl T and Schneider C M 2002 *J. Appl. Phys.* **91** 7026
[29] Jensen A, Hauptmann J R, Nygard J and Lindelof P E 2005 *Phys. Rev.* B **72** 035419
[30] Sahoo S, Kontos T, Furer J, Hoffmann C, Gräber M, Cottet A and Schönenberger C 2005 *Nat. Phys.* **1** 102
[31] Pasupathy A N, Bialczak R C, Martinek J, Grose J E, Donev L A K, McEuen P L and Ralph D C 2004 *Science* **306** 86

[32] Bernand-Mantel A, Seneor P, Lidgi N, Munoz M, Cros V, Fusil S, Bouzehouane K, Deranlot C, Vaures A, Petroff F and Fert A 2006 *Appl. Phys. Lett.* **89** 062502
[33] Sasaki S, De Franceschi S, Elzerman J M, van der Wiel W G, Eto M, Tarucha S and Kouwenhoven L P 2000 *Nature* **405** 764
[34] Kogan A, Amasha S, Goldhaber-Gordon D, Granger G, Kastner M A and Shtrikman H 2004 *Phys. Rev. Lett.* **93** 166602
[35] Averin D V and Odintsov A A 1989 *Phys. Lett.* A **140** 251
     Averin D V and Nazarov Yu V 1990 *Phys. Rev. Lett.* **65** 2446
     Kang K and Min B I 1997 *Phys. Rev.* B **55** 15412
[36] Schoeller H and Schön G 1994 *Phys. Rev.* B **50** 18436
     König J, Schmid J, Schoeller H and Schön G 1996 *Phys. Rev.* B **54** 16820
     König J 1999 *Quantum Fluctuations in the Single-Electron Transistor* (Aachen: Shaker)
[37] Thielmann A, Hettler M H, König J and Schön G 2003 *Phys. Rev.* B **68** 115105
[38] Thielmann A, Hettler M H, König J and Schön G 2006 *Phys. Rev. Lett.* **95** 146806
[39] Barnaś J, Martinek J, Michałek G, Bułka B R and Fert A 2000 *Phys. Rev.* B **62** 12363
[40] Blanter Ya M and Büttiker M 2000 *Phys. Rep.* **336** 1
[41] Sukhorukov E V, Burkard G and Loss D 2001 *Phys. Rev.* B **63** 125315
[42] Cottet A, Belzig W and Bruder C 2004 *Phys. Rev.* B **70** 115315
     Cottet A, Belzig W and Bruder C 2004 *Phys. Rev. Lett.* **92** 206801
[43] Weymann I and Barnaś J 2006 *Phys. Rev.* B **73** 205309
[44] Weinmann D, Husler W and Kramer B 1995 *Phys. Rev. Lett.* **74** 984
[45] Fransson J and Rasander M 2006 *Phys. Rev.* B **73** 205333
     Fransson J 2006 *New J. Phys.* **8** 114
[46] Ono K, Austing D G, Tokura Y and Tarucha S 2002 *Science* **297** 1313